Ultrasonics 92 (2019) 1–7

Contents lists available at ScienceDirect

Ultrasonics

journal homepage: www.elsevier.com/locate/ultras

Fractional-order Darwinian PSO-based feature selection for media-adventitia border detection in intravascular ultrasound images

Yuan-Yuan Wang[a,b], Wen-Xian Peng[c], Chen-Hui Qiu[a,b], Jun Jiang[d], Shun-Ren Xia[a,b,*]

[a] Key Laboratory of Biomedical Engineering of Ministry of Education Zhejiang University, China
[b] Zhejiang Provincial Key Laboratory of Cardio-Cerebral Vascular Detection Technology and Medicinal Effectiveness Appraisal Zhejiang University, China
[c] Radiology Department of Hangzhou Medical College, China
[d] Second Affiliated Hospital, Zhejiang University School of Medicine, China

ARTICLE INFO

Keywords:
Intravascular ultrasound image
Border detection
Multi-classification
Feature selection
Fractional calculus

ABSTRACT

Media-adventitia (MA) border delineates the outer appearance of arterial wall in intravascular ultrasound (IVUS) image. The detection of MA border is a challenging topic due to many difficulties such as complicated intravascular structures, intrinsic artifacts and image noises. We propose a classification-based MA border detection method with an embedded feature selection technique. The feature selection technique is based on Fractional-order Darwinian particle swarm optimization (FODPSO) algorithm. By employing feature selection, 293-dimension features including multi-scale features, gray-scale features and morphological feature are reducing to 37-dimension. The border detection method with feature selection is tested on a public dataset extracted from in-vivo pullbacks of human coronary arteries, which contains 77 IVUS images. Three indicators, Jaccard (JACC), Hausdorff Distance (HD) and Percentage of Area Difference (PAD), are measured for quantitative evaluation. Detection with 293-dimension features obtains JACC 0.79, HD 1.41 and PAD 0.16, while detection with 37-dimension features obtains JACC 0.83, HD 1.27 and PAD 0.12, indicating that the FODPSO-based feature selection method improves MA border detection by JACC 0.04, HD 0.14 and PAD 0.04. Furthermore, the proposed border detection method acquires better performances compared with two other automatic methods conducted on the same dataset available in literature.

1. Introduction

Atherosclerosis is one of the deadliest diseases for pathological reasons (stenosis, vulnerable plaque, etc.) and diagnostic failures [1]. Intravascular ultrasound (IVUS) is viewed as the ground truth for atherosclerosis diagnosis and interventional therapy, which provides real-time cross-sectional images of vessels through pulling back catheter from the distal end of artery. Media-adventitia (MA) border delineates the outer appearance of artery. Extracting MA border is an essential step for calculating plaque burden and diagnosing atherosclerosis.

Many factors obstruct MA border detection such as complicated intravascular structures, intrinsic artifacts and image noises. Many structures (lumen, plaque, calcification, imaging shadow, etc.) exist in IVUS images, and affect MA border detection in their own ways. For instances, calcification lays inside MA border, exterior area lays outside MA border, imaging shadow and guide wire artifact lay inside, on or outside MA border. Lots of approaches adopted these structure information in the MA border detection procedure [2,3]. Literature [3] proposed a region selection strategy which relaxed the segmentation of lumen and MA border to assign two nested ERELs for lumen and media. EREL is a recently proposed region detector, namely Extremal Region of Extremum Level [4]. Classification-based MA border detection in literatures [5–9] separated structures and detected MA border according to each structure's effect. Gray level probability density function was adopted to classify images, and fast-marching method was employed to locate lumen and MA border in [5,7]. Literature [6] presented a holistic approach which detected MA border by learning the relationships between different tissues. Binary classification results were obtained by an artificial neural network [8], five structures were distinguished by support vector machine [9], and deformable model was employed to get borders based on these classification results [8,9].

To obtain such classified results, various features have been introduced, i.e. intensity [10], texture features [11,12], spectral features [13,14], customized shadow-related features [15]. Due to the complexity of IVUS images, many features could be involved to obtain

* Corresponding author at: The Key Lab of Biomedical Engineering of Ministry of Education, Zhejiang University, ZheDa Road 38th, Hangzhou 310027, China.
E-mail address: corresponding_xia@163.com (S.-R. Xia).

https://doi.org/10.1016/j.ultras.2018.06.012
Received 26 December 2017; Received in revised form 25 May 2018; Accepted 16 June 2018
Available online 18 June 2018
0041-624X/

accurate classification results. Employing too many features in classification problems may lead to lower computation accuracy, slower speed and additional memory occupation. Feature selection is used to choose smaller feature subsets, and to improve the predicting accuracy in the meantime.

Most feature selection algorithms contain an optimization procedure to find the optimal solution under some criteria. Particle swarm optimization (PSO) [16] is an extremely simple yet fundamentally effective optimization algorithm, and has produced encouraging results in feature selection [17,18]. Multi-objective PSO was firstly applied by considering feature selection as a multi-objective optimization problem [19]. Some improved PSO such as hybridization of genetic algorithm (GA) and PSO [20], and fractional-order Darwinian particle swarm optimization (FODPSO) algorithm [21], were introduced and both achieved good performance in feature selection.

Considering the difficulties in MA border detection, it's quite benefit to distinguish each structure in IVUS images before MA border detection. In this study, 293-dimension features are firstly constructed for IVUS image classification. Then, a FODPSO-based feature selection method is proposed to select the most effective feature subset. Compared with original PSO, FODPSO can effectively avoid trapping into local optimum, due to its advantages of controlling convergence speed and extending PSO by natural selection. FODPSO-based feature selection method reduces the feature subset to 37-dimension. Based on the classification results, a new external force field is constructed in a Snake model to detect MA border through curve evolution.

2. Materials and methods

2.1. IVUS image sources

Literature [22] provides two public dataset, named set A and set B, acquired by 40 MHz and 20 MHz catheter probes, respectively. Dataset A in 40 MHz is adopted in our work. The dataset contains a set of 77 images from 22 patients in rectangular coordinate, size 512×512. The first 19 images constitute the training set, and the rest 58 ones are the testing set. Many complex situations such as bifurcation, shadow artifact and side vessels are involved in the adopted dataset, which makes the MA border detection more challenging. Considering complexity and diversity of the dataset, two clinical experts delineate three sets of ground truth [22]. This annotation is double-blind and one of the experts repeated labeling after about one week from the first annotation.

2.2. Features involved

A classification-based border detection method is employed to extract MA border in IVUS images. In order to better detect MA border, a multi-class Extreme Learning Machine (ELM) [23] model is adopted to classify IVUS image into nine classes: catheter, blood, plaque, adventitia, external tissues, calcification, shadow, guide wire artifacts, MA border. Clinical experts manually annotate nine or less regions for every image in the training set. 200 pixels per class per image are selected, constructing a sufficient training set. Example of IVUS image in the training set and its annotations are depicted in Fig. 1.

Before extracting features, IVUS images are transformed to polar coordinate. Column and row in polar image represent the tangential and radial resolutions of scanning, respectively. Thus, size of polar image is set to 256 by 360. We extract 293-dimension features including multi-scale features, gray-scale features and morphological feature. Details about these features are listed in Table 1.

2.3. Fractional-order Darwinian PSO based feature selection method

Feature selection technique aims at reducing the size of feature subset and improving the classification accuracy meanwhile. For the 293-dimension features, we assign a weight parameter θ for each feature, $\theta \in [-1, 1]$. One feature is abandoned when its corresponding θ is less than 0, otherwise the feature is selected. The fitness function is set to the classification accuracy acquired by ELM in the training set. An improved particle swarm optimization (PSO) algorithm is utilized to find the optimal solutions.

PSO searches the optimal solutions of fitness function using a swarm of particles. Each particle updates its moving direction according to the best position of itself (pbest) and the best position of the whole swarm (gbest), formulated as:

$$V_i(t+1) = \omega V_i(t) + c_1 r_1 (P_p - X_i(t)) + c_2 r_2 (P_g - X_i(t)) \quad (1)$$

$$X_i(t+1) = X_i(t) + V_i(t+1) \quad (2)$$

where V_i is the moving velocity at generation i, X_i is the particle position. P_p denotes pbest, P_g denotes gbest. ω, c, r denote the inertia weight, learning factors and random numbers respectively.

Darwinian particle swarm optimization (DPSO) runs many parallel PSO simultaneously to avoid being trapped in local optimum like single PSO [24]. Each PSO, called a swarm, searches optimum like an ordinary PSO. Each swarm evolves under certain rules: extend swarm life when a new global optimum is found in the swarm, otherwise swarm life is reduced or even deleted. DPSO has been proven to be superior to original PSO in escaping local optimum [24].

Fractional-order particle swarm optimization (FOPSO) controls the convergence rate by introducing fractional calculus in particles' velocity [25]. Eq. (1) is deformed with $\omega = 1$, namely:

$$V_i(t+1) - V_i(t) = c_1 r_1 (P_p - X_i(t)) + c_2 r_2 (P_g - X_i(t)) \quad (3)$$

The left side $V_i(t+1) - V_i(t)$ is a discrete version of $D^{\alpha}[v_{t+1}]$ with $\alpha = 1$. $D^{\alpha}[v_{t+1}]$ denotes the derivative of velocity. The Grünwald–Letnikov derivative can be implemented as:

$$D^{\alpha}[v_t] = \frac{1}{T^{\alpha}} \sum_{k=0}^{r} (-1)^k \Gamma(\alpha+1) v(t-kT) / \Gamma(k+1)\Gamma(\alpha-k+1) \quad (4)$$

where T is the sample period and $r$is the truncate order. Bring Eq. (4) into Eq. (3) with $r = 4$, yielding Eq. (5):

$$V_i(t+1) = \alpha V_i(t) + \frac{\alpha}{2} V_i(t-1) + \frac{\alpha(1-\alpha)}{6} V_i(t-2) + \frac{\alpha(1-\alpha)(2-\alpha)}{24} V_i(t-3) + c_1 r_1 (P_p - X_i(t)) + c_2 r_2 (P_g - X_i(t)) \quad (5)$$

Introduce Eq. (5) to update each particle's velocity in DPSO, generating a new algorithm named as Fractional-order Darwinian particle swarm optimization (FODPSO) [26]. FODPSO is proven to be superior to FOPSO and DPSO in the ability of searching global optimum [26].

FODPSO is used to find the optimal solution of fitness function constructed by classification accuracy, obtaining a 37-dimension feature subset.

2.4. Border detection procedure

The MA border detection procedure is depicted in Fig. 2. The classified IVUS images are transformed into rectangular coordinate, which is convenient for Snake model [27] to evolve. The classified IVUS image is shown in Fig. 3(a). A new external force field is constructed by adding a bias to the original one. The bias is formed by the classification results. For those pixels which are classified as catheter, blood, plaque and calcification, a unit force pointing away from the center is added. For those pixels which are classified as adventitia, external tissues, a unit force pointing to the center is added. The force field is shown in Fig. 3(b). The initial curve evolves under the specified force field in a gradient vector flow (GVF) Snake model [28]. The evolution stops when the iterations reach the maximum number of iterations. A balloon force [29] is added to make the curve have a more dynamic behavior.

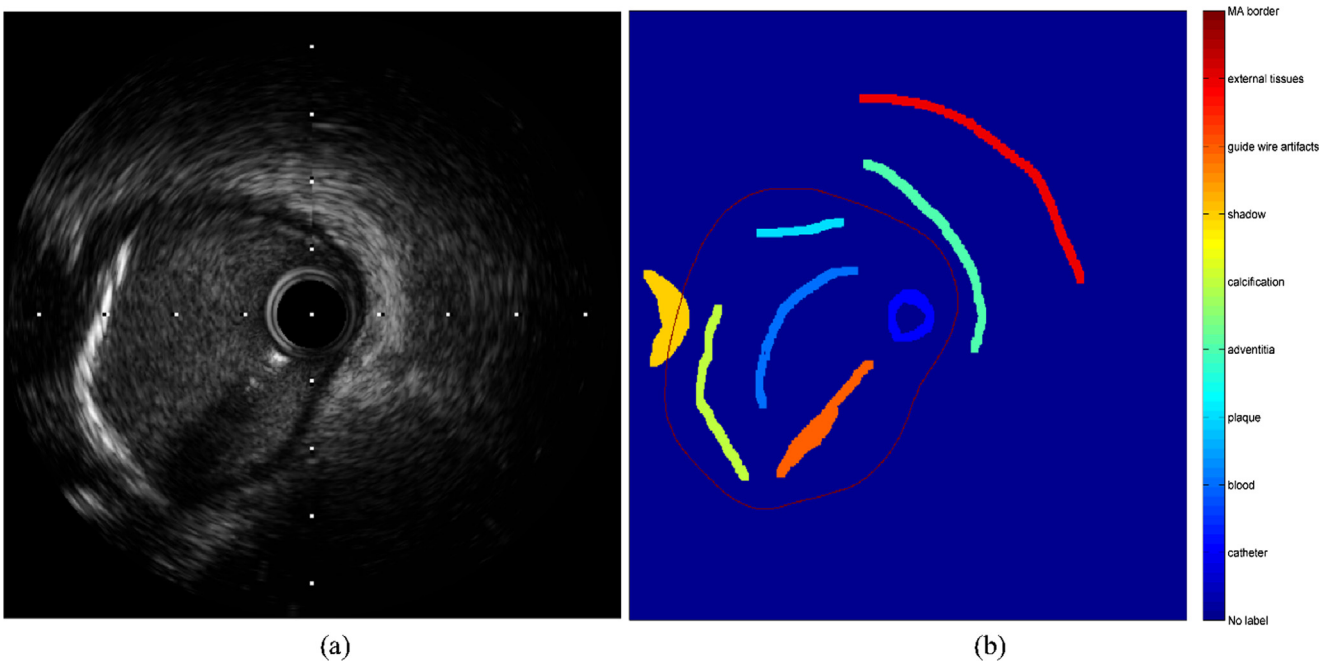

Fig. 1. (a) Example IVUS image in the training set. (b) Nine regions manually annotated by experts.

3. Results and discussion

Feature selection and border detection are the main two steps, corresponding to FODPSO and Snake model, respectively. Parameter setting about these two algorithms are listed in Table 2, according to related literatures. We run FODPSO for 10 independent times to gain relatively stable feature subsets. α in Eq. (5) is formulated by Eq. (6), where N denotes the number of iteration.

$$\alpha = 0.8-0.4 \times (t/N),\ t = 1, 2, \cdots, N \tag{6}$$

Four images with detected border and ground truth are shown in Fig. 4, in which dotted line denotes detected border while solid line denotes ground truth delineated by experienced doctor. The detected border matches the ground truth well in most situations. Three indicators, Jaccard (JACC), Hausdorff Distance (HD) and Percentage of Area Difference (PAD), formulated in literature [22], are measured for quantitative evaluation of the detected border against three sets of ground truth. Larger JACC is preferred, while smaller PAD and HD are preferred.

To evaluate the necessity of the proposed classification-based MA border detection approach, we adopt GVF Snake model on IVUS images directly, and obtain three indicators i.e. JACC 0.64 (0.14), HD 2.30 (1.12) and PAD 0.50 (0.46). Classical GVF snake model employs image gradient to evolve curve, and performs well in simple detection of edges, lines and contours. However, employing GVF snake model on IVUS images directly cannot detect satisfactory results of MA border. Firstly, many noise and artifacts exist in IVUS images, which can produce disturbing force filed even in the homogeneous regions. Secondly,

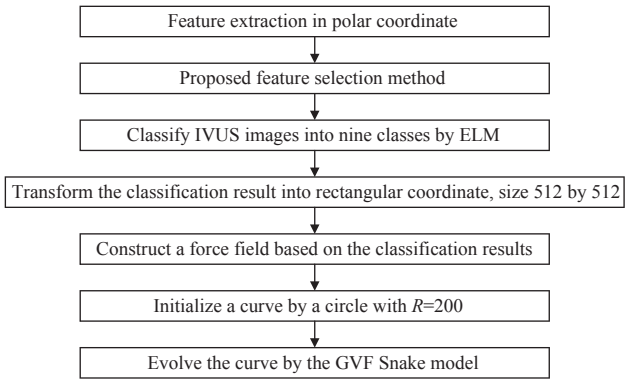

Fig. 2. Flowchart of the procedure of MA border detection.

Table 1
Details about original features and selected features.

Features categories	Features' details	Number	Selected
Multi-scale features	Contourlet transform [32], size 16 × 16	1–256	1, 2, 3, 4, 7, 8, 9, 11, 12, 13, 14, 15, 16, 129, 132, 136, 259, 262, 263,
Gray-scale features	3 × 3 Sobel operator	257	264, 265, 266, 267, 268, 280, 281, 282, 283, 284, 286, 287, 288, 289,
	3 × 3 averaging operator	258	290, 291, 292, 293
	Mean value, standard deviation and their ratio in a sliding window of size 3 × 5 along radial and angular axes [6]	259–264	
	Shadow and relative shadow [6,15]	265, 266	
	Modified gray filter [30]	267	
	First-order and second-order derivative of Gaussian operator in four directions, with σ = 2	268–275	
	Four parameters (autocorrelation, energy, entropy, sum average) in four directions of 7 × 7 Gy-level co-occurrence matrixes [15]	276–291	
	Local contrast variation by a 9 × 9 mask	292	
Morphological feature	Relative position of each structure referring to MA border, see Appendix A	293	

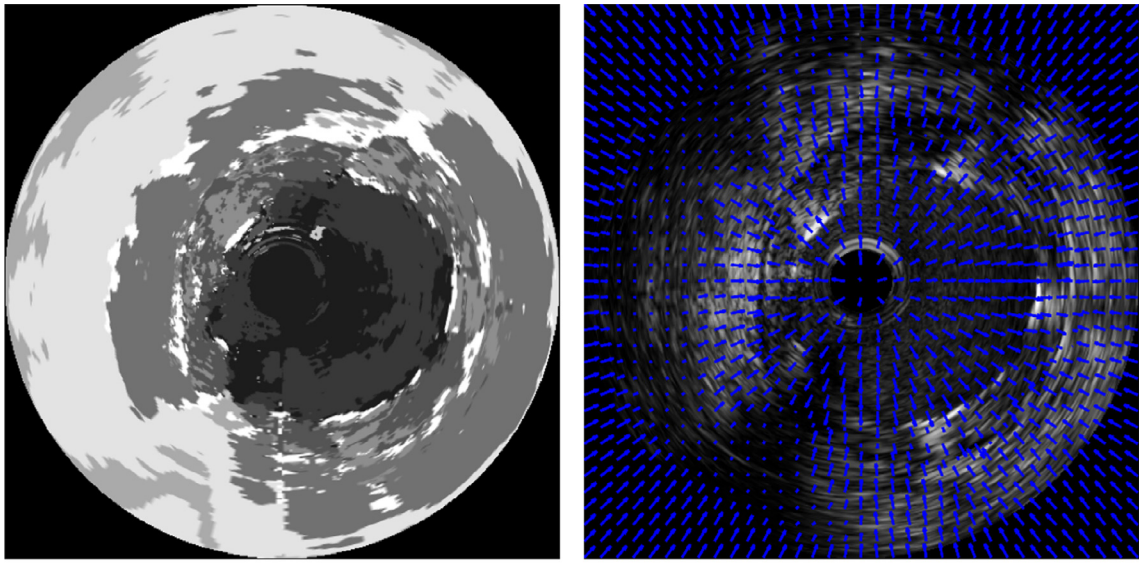

Fig. 3. The classified image and the external force field constructed by the classification result.

Table 2
Parameter setting in FODPSO and Snake.

FODPSO		Snake	
Number of iteration	50	Weight of first order	1
Number of swarm	5	Weight of second order	1
Population	20	Weight of external image force	0.8
c_1	0.8	Balloon force	0.2
c_2	0.8	Number of iterations	600

IVUS images contain lots of structures and abundant detail information, which may lead a disordered external force field. Based on the above reasons, a bias force based on classification results is added to the original GVF force field. The proposed classification-based framework improves MA border detection, demonstrates its necessity and effectiveness.

All these 293-dimension features provide more or less information for classification. For examples, the shadow and relative shadow features can identify most shadow areas in image, the modified gray filter feature aims at recognizing MA border location, and the morphological feature represents the relative position of each structure to MA border. According to Table 1, such discriminating features are selected by the FODPSO-based feature selection method. On the contrary, some features such as Sobel operator and averaging operator, which provide less information for classification, are excluded by the feature selection method. Through the FODPSO-based feature selection method, 37-dimension features are selected.

In order to evaluate the proposed feature selection method, we employ 37-dimension features selected by FODPSO-based feature selection method, 80-dimension features selected by ReliefF feature selection method, and 293-dimension features without any feature selection method in the MA border detection process. Three indicators are calculated among the three experiments, and the statistical results are shown in Table 3. Boxplot about the three experiments are depicted in Fig. 5. ReliefF is a feature weighting algorithm, by which we attempt to employ the most important 30, 80, 120, 180 features in MA border detection, and employing 80 features obtains the best performance. Therefore, 80-dimension features selected by ReliefF feature selection method are used as comparison.

According to Table 3, border detection method with the proposed FODPSO-based feature selection improves JACC 0.04, HD 0.14 and PAD 0.04, compared with adopting 293-dimension features, and improves JACC 0.01, HD 0.08 and PAD 0.02, compared with adopting 80-dimension features. Meanwhile, the proposed feature selection method acquires the smallest standard value among three experiments. Fig. 5 demonstrates this superiority in a more straightforward approach. Smaller IQR in boxplot means that experiment with feature selection owns less dispersion.

In order to evaluate the MA border detection method with feature selection more objectively, it is compared with three other methods, label as P3, P6 and P8 in literature [21]. The statistical results are shown in Table 4. The results of P3, P6 and P8 are taken from Row Media-A; Column P3, P6, P8 of Table 5 in literature [21]. P3 adopts a mixture model of four gamma statistical distributions for image classification, and a fast-marching method for curve evolution. P6 is a holistic approach, which considers MA border as a part of the whole vessel, and detects MA border by learning relationships among all tissues. P8 computes MA border in a frame using the information of former frame.

Among all the comparing methods, P8 employs sequential information, while P3, P6 and the proposed method only use the information in the current frame. P3 is semi-automatic method, while P6, P8 and the proposed one are automatic methods. Overall, P3 performs better than P8, and P8 performs better than P6. The proposed MA border detection procedure gets similar performance with P6 when employing the whole 293-dimension feature set. Through the proposed FODPSO-based feature selection, 293-dimension feature set is reduced to 37-dimension feature subset. The proposed method embedded feature selection obtains JACC 0.83, HD 1.27, and PAD 0.12, which obtains the second best results among all the comparative methods, and the best ones among the automatic methods. It indicates that FODPSO-based feature selection improves the MA border detection largely.

Effective features are the key points in image classification. Most of the 293-dimension features are extracted for IVUS images acquired from 40 MHz probes. Some features like the modified gray filter feature and the morphological feature are specialized for MA border. Thus the proposed method achieves good performance when detecting MA border in IVUS images of 40 MHz. More features should be explored when detecting lumen border or IVUS images of 20 MHz. The running time of the proposed method mainly relies on the speed of feature extraction, since the computational speed of ELM and Snake are quite fast, and FODPSO-based feature selection method doesn't run for each image

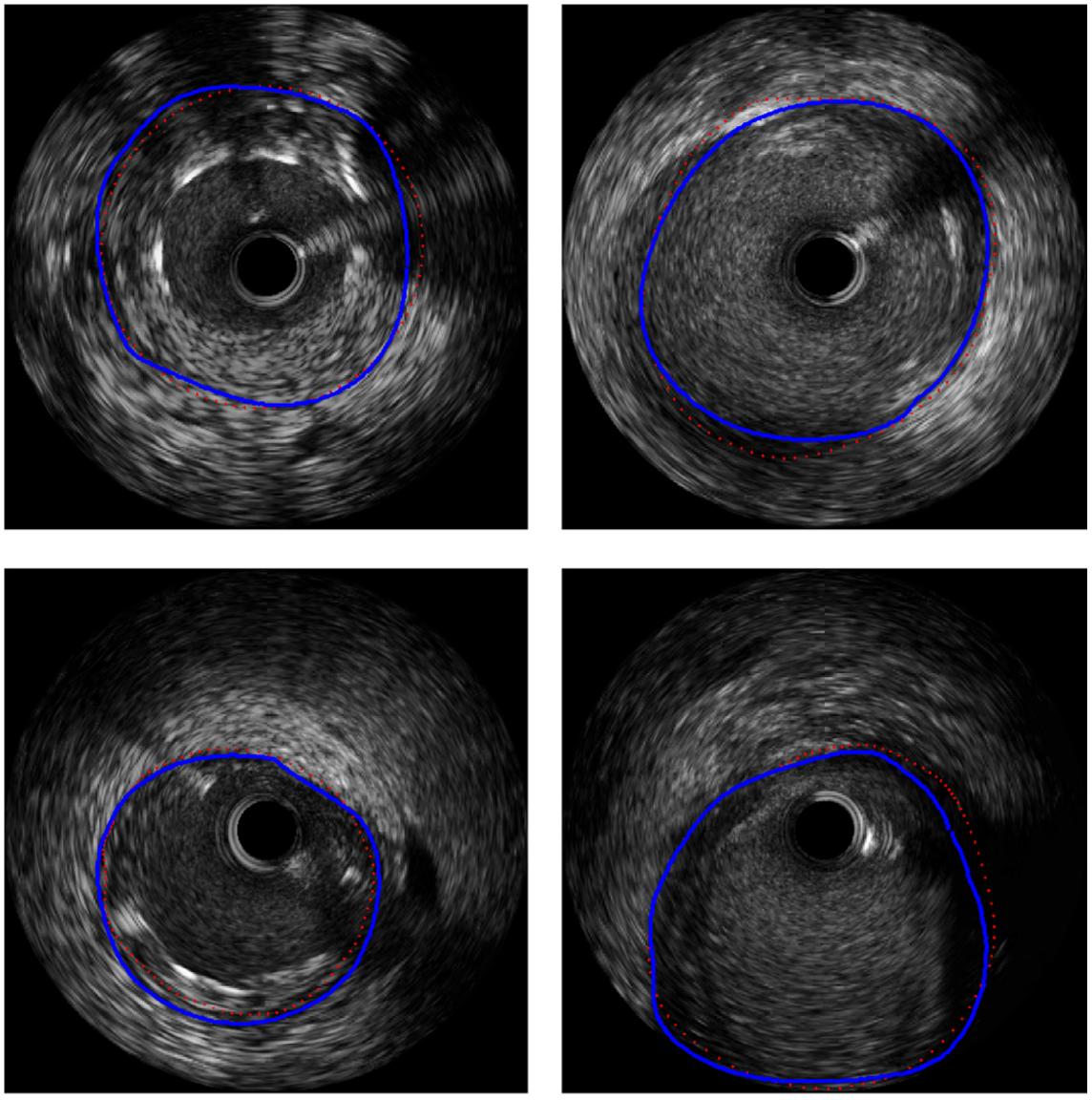

Fig. 4. MA border detection results, depicted as dotted line and ground truth depicted in solid line.

Table 3
Statistical analysis of three experiments. Method A1 denotes "Without feature selection", method A2 denotes "With ReliefF feature selection", method A3 denotes "With FODPSO-based feature selection". Format is set as mean value (standard value).

Method	Indicator		
	JACC	HD	PAD
A1	0.79 (0.10)	1.41 (0.67)	0.16 (0.18)
A2	0.82 (0.13)	1.35 (0.78)	0.14 (0.16)
A3	**0.83 (0.09)**	**1.27 (0.67)**	**0.12 (0.13)**

in the testing set. In practice, we construct a feature database for each image in the training set and testing set. The average running time of feature extraction for one image is 272.92 s (Core 4, 2.67 GHz). We select the corresponding features from the database in border detection process to make this process more efficient.

4. Conclusions

Many structures, affecting MA border detection in different ways, exist in IVUS images. To classify each structure, we extract 293-dimension features including multi-scale features, gray-scale features and morphological feature. A FODPSO-based feature selection method is applied to reduce the feature dimension and increase the classification accuracy. FODPSO is an intelligent optimization algorithm which owns better global search ability than PSO. By this feature selection method, 293-dimension features are reduced to 37-dimension.

MA border is detected based on the multi-classification results. The MA border detection is evaluated by three indicators: JACC, HD and PAD. Adopting the selected 37-dimension features improves three indicators by JACC 0.04, HD 0.14 and PAD 0.04, compared with adopting 293-dimension features. Comparative experiments with two other border detection methods are implemented, the proposed one achieves the best three indicators among all the automatic methods, which demonstrates its effectiveness.

5. Declarations of interest

None

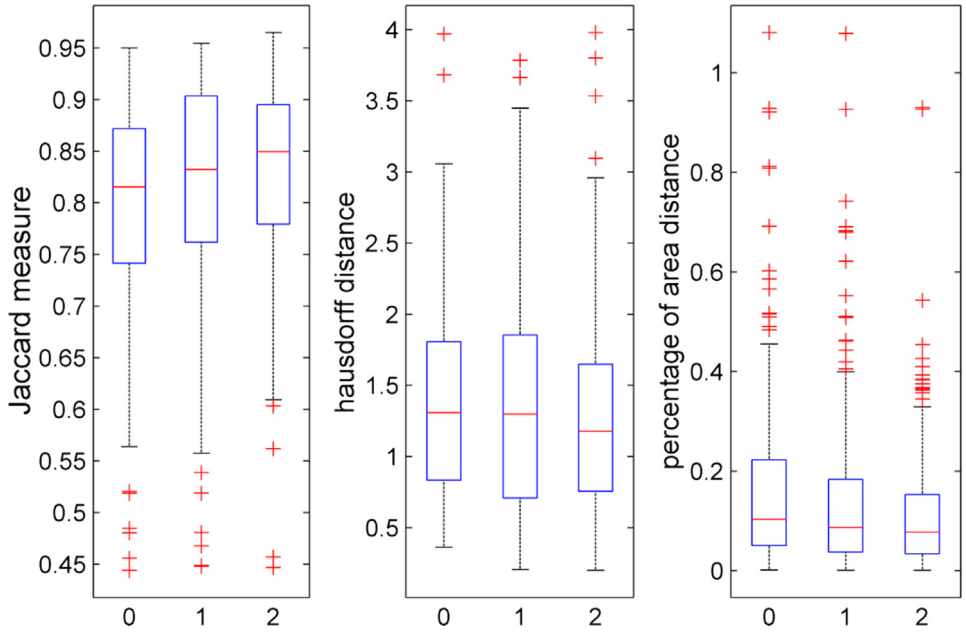

Fig. 5. Boxplot of three indicators in three experiments (0 denotes experiment without feature selection; 1 with classic ReliefF feature selection; 2 with FODPSO-based feature selection).

Table 4
Statistical comparison with other methods. Format is set as mean value (standard value).

Method	Indicator			Auto/Semi
	JACC	HD	PAD	
P3	**0.86 (0.11)**	**1.18 (1.02)**	**0.10 (0.11)**	Semi
P6	0.76 (0.11)	1.78 (0.83)	0.17 (0.14)	Auto
P8	0.80 (0.13)	1.57 (1.03)	0.14 (0.16)	Auto
Proposed	0.83 (0.09)	1.27 (0.67)	0.12 (0.13)	Auto

Acknowledgements

The authors first sincerely thank the editors and anonymous reviewers for their constructive comments and suggestions. The authors would also like to sincerely thank Dr. Simone Balocco from University of Barcelona (Spain) for providing the dataset. This work is supported by Research and Development (No. 2016YFC1306600).

Appendix A

The procedure of generating the morphological feature which defines the relative position of each structure referring to MA border is depicted in the following flowchart, in which the energy function is calculated by adding the normalized IVUS image, a gradient image calculated by modified gray filter [30], and a border image detected by combination of receptive fields [31] together. In this morphological feature, each pixel gets its value by multiplying its Euclidean distance to the fitting curve and a sign number (-1 for those pixels inside the fitting curve, 1 for those outside the curve) together.

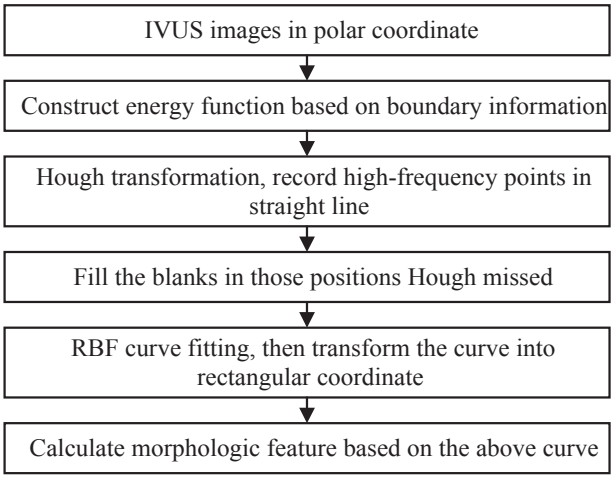

Appendix B. Supplementary material

Supplementary data associated with this article can be found, in the online version, at https://doi.org/10.1016/j.ultras.2018.06.012.

References

[1] A. Katouzian, E.D. Angelini, S.G. Carlier, J.S. Suri, N. Navab, A.F. Laine, A state-of-the-art review on segmentation algorithms in intravascular ultrasound (IVUS) images, IEEE Trans. Inform. Technol. Biomed. 16 (2012) 823–834.
[2] F. Destrempes, M.R. Cardinal, L. Allard, J.-C. Tardif, G. Cloutier, Segmentation method of intravascular ultrasound images of human coronary arteries, Comput. Med. Imaging Graph. 38 (2014) 91–103.
[3] M. Faraji, I. Cheng, I. Naudin, A. Basu, Segmentation of arterial walls in intravascular ultrasound cross-sectional images using extremal region selection, Ultrasonics 84 (2017) 356–365.
[4] M. Faraji, J. Shanbehzadeh, K. Nasrollahi, T. Moeslund, Extremal regions detection guided by maxima of gradient magnitude, IEEE Trans. Image Process. 24 (2015) 5401–5415.
[5] M.R. Cardinal, G. Soulez, J.C.T.J. Meunier, G. Cloutier, Fast-marching segmentation of three-dimensional intravascular ultrasound images: a pre-and post-intervention study, Med. Phys. 37 (2010) 3633–3647.
[6] F. Ciompi, O. Pujol, C. Gatta, M. Alberti, S. Balocco, X. Carrillo, J. Mauri-Ferre, P. Radeva, HoliMAb: a holistic approach for media–adventitia border detection in intravascular ultrasound, Med. Image Anal. 16 (2012) 1085–1100.
[7] M.R. Cardinal, J. Meunier, G. Soulez, R.L. Maurice, E. Therasse, G. Cloutier, Intravascular ultrasound image segmentation: a three-dimensional fast-marching method based on gray level distributions, IEEE Trans. Med. Imaging 25 (2006) 590–601.
[8] S. Su, Z. Hu, Q. Lin, W.K. Hau, Z. Gao, H. Zhang, An artificial neural network method for lumen and media-adventitia border detection in IVUS, Comput. Med. Imaging Graph. 57 (2017) 29–39.
[9] F. Chen, R. Ma, J. Liu, M. Zhu, H. Liao, Lumen and media-adventitia border detection in IVUS images using texture enhanced deformable model, Comput. Med. Imaging Graph. 66 (2018) 1–13.
[10] E.G. Mendizabal-Ruiz, M. Rivera, I.A. Kakadiaris, Segmentation of the luminal border in intravascular ultrasound B-mode images using a probabilistic approach, Med. Image Anal. 17 (2013) 649–670.
[11] V.G. Giannoglou, J.B. Theocharis, Decision fusion of multiple classifiers for corollary plaque characterization from IVUS images, Int. J. Artif. Intell. Tools 23 (2014) 1–29.
[12] X. Zhang, C.R. McKay, M. Sonka, Tissue characterization in intravascular ultrasound images, IEEE Trans. Med. Imaging 17 (1998) 889–899.
[13] F. Ciompi, O. Pujol, C. Gatta, O. Rodríguez-Leor, J. Mauri-Ferré, P. Radeva, Fusing in-vitro and in-vivo intravascular ultrasound data for plaque characterization, Int. J. Cardiovasc. Imaging 26 (2010) 763–779.
[14] A. Nair, B.D. Kuban, E.M. Tuzcu, P. Schoenhagen, S.E. Nissen, D.G. Vince, Coronary plaque classification with intravascular ultrasound radiofrequency data analysis, Circulation 106 (2002) 2200–2206.
[15] K.L. Caballero, J. Barajas, O. Pujol, O. Rodriguez, P. Radeva, Using reconstructed IVUS images for coronary plaque classification, in: Engineering in Medicine and Biology Society, 29th Annual International Conference of the IEEE 2007, pp. 2167–2170.
[16] J. Kennedy, Particle swarm optimization, in: Encyclopedia of Machine Learning, Springer, 1995, pp. 760–766.
[17] L. Shang, Z. Zhou, X. Liu, Particle swarm optimization-based feature selection in sentiment classification, Soft. Comput. 20 (2016) 1–14.
[18] H.B. Nguyen, B. Xue, I. Liu, P. Andreae, M. Zhang, New mechanism for archive maintenance in PSO-based multi-objective feature selection, Soft. Comput. 10 (2016) 1–20.
[19] B. Xue, M. Zhang, W.N. Browne, Particle swarm optimization for feature selection in classification: a multi-objective approach, IEEE Trans. Cybern. 43 (2013) 1656–1671.
[20] P. Ghamisi, J.A. Benediktsson, Feature selection based on hybridization of genetic algorithm and particle swarm optimization, IEEE Geosci. Remote Sens. Lett. 12 (2015) 309–313.
[21] P. Ghamisi, M.S. Couceiro, J.A. Benediktsson, A novel feature selection approach based on FODPSO and SVM, IEEE Trans. Geosci. Remote Sens. 53 (2015) 2935–2947.
[22] S. Balocco, C. Gatta, F. Ciompi, A. Wahle, P. Radeva, S. Carlier, G. Unal, E. Sanidas, J. Mauri, X. Carillo, T. Kovarnik, C.-W. Wang, H.-C. Chen, T.P. Exarchos, D.I. Fotiadis, F. Destrempes, G. Cloutier, O. Pujol, M. Alberti, E.G. Mendizabal-Ruiz, M. Rivera, T. Aksoy, R.W. Downe, I.A. Kakadiaris, Standardized evaluation methodology and reference database for evaluating IVUS image segmentation, Comput. Med. Imaging Graph. 38 (2014) 70–90.
[23] G.B. Huang, Q.Y. Zhu, C.K. Siew, Extreme learning machine: theory and applications, Neurocomputing 70 (2006) 489–501.
[24] J. Tillett, T. Rao, F. Sahin, R. Rao, Darwinian particle swarm optimization, in: Indian International Conference on Artificial Intelligence, Pune, India, December. DBLP 2005, pp. 1474–1487.
[25] E. Solteiro Pires, J. Tenreiro Machado, P. de Moura Oliveira, J. Boaventura Cunha, L. Mendes, Particle swarm optimization with fractional-order velocity, Nonlinear Dyn. 61 (2010) 295–301.
[26] M.S. Couceiro, R.P. Rocha, N.M.F. Ferreira, J.A.T. Machado, Introducing the fractional-order Darwinian PSO, SIViP 6 (2012) 1–8.
[27] M. Kass, A. Witkin, D. Terzopoulos, Snakes: active contour models, Int. J. Comput. Vision 1 (1988) 321–331.
[28] C. Xu, J.L. Prince, Snakes, shapes, and gradient vector flow, IEEE Trans. Image Process. 7 (1998) 359–369.
[29] L.D. Cohen, On active contour models and balloons, CVGIP: Image Understand. 53 (1991) 211–218.
[30] G. Unal, S. Bucher, S. Carlier, G. Slabaugh, T. Fang, K. Tanaka, Shape-driven segmentation of the arterial wall in intravascular ultrasound images, IEEE Trans. Inform. Technol. Biomed. (2008) 335–347.
[31] G. Azzopardi, N. Petkov, A CORF computational model of a simple cell that relies on LGN input outperforms the Gabor function model, Biol. Cybern. 106 (2012) 177–189.
[32] D.Y. Po, M.N. Do, Directional multiscale modeling of images using the contourlet transform, IEEE Trans. Image Process. A Public. IEEE Signal Process. Soc. 15 (2006) 1610–1620.